Stress Intensity Factors for Arbitrarily Located and Oriented Cracks in a Cylindrical Shell with Tori-Spherical End Closures subjected to Internal Pressure

Shivashankar R Srivatsa*, H V Lakshminarayana*, Pramod R**

*(Department of Mechanical Engineering, Dayananda Sagar College of Engineering, Kumaraswamy Layout, Bangalore 560078, India)
**(Department of Mechanical Engineering, Amrita School of Engineering, Kasavanahalli, Bangalore 560035, India.

ABSTRACT

A refined finite element model and a new post processing subprogram to determine mixed mode membrane and bending stress intensity factors for arbitrarily located and oriented cracks in complex shell type structures is presented. A fine mesh of singular isoparametric triangular shell element (STRIA6) with user specified number NS from one crack face to another and size Δa is created around each crack-tip. The rest of the domain is discretized using a compatible mesh of regular quadratic isoparametric triangular shell element (TRIA6) and quadratic isoparametric quadrilateral shell element (QUAD8). A new post processing subprogram 3MBSIF is presented to compute the Stress Intensity Factors Posteriori. The proposed Finite Element Model implemented using ABAQUS, a unified FEA software, and the new post processing subprogram 3MBSIF are validated using benchmarks, a set of standard test problems with known target solutions. Selected results of a parametric study are presented for arbitrarily oriented cracks of increasing lengths in the toroidal segment of a cylindrical shell with tori-spherical end closures under internal pressure loading.

Keywords - Finite Element, Membrane & Bending SIF, Mixed Mode Fracture, Post processing subprogram, Torispherical shell

I. INTRODUCTION

Cracks are unavoidable in the construction and operation of aerospace structures, pressure vessels, piping components, thermal and nuclear power plant components. This fact is significant because fracture of these components begins at crack tips. Hence a crack can trigger a local failure at a load level lower than the global failure load of a corresponding shell structure without a crack. As a result critical assessment of structural integrity (stiffness, strength, durability) is often based on Fracture Mechanics Analysis. Therefore, an accurate determination of crack-tip stress intensity factor in a given shell structure subjected to various types of loading and support conditions is essential to the development of safe and reliable designs. Moreover, validated finite element models created using commercial FEA software would be very valuable to structural designers for the development of innovative damage tolerant design concepts.

An up-to-date survey of methods of analysis and stress intensity factor solutions to crack problems in shell structures is presented by Raju et al.[1]. The solution methods can be grouped into three major categories:

A. Continuum Mechanics methods
    Differential equation approach
    Integral equation approach
B. Numerical methods
    Finite Element Method
    Boundary element method
C. Experimental methods
    Photo elasticity and caustics
    Holographic Interferometry

Most of the previous studies are limited to specific geometries such as cylindrical, spherical and axisymmetric shells. The problem of arbitrarily located and oriented cracks in a cylindrical shell with tori-spherical end closures is intractable by continuum mechanics methods. Experimental investigations are prohibitively expensive and time consuming. Therefore, Finite Element Modelling using commercial FEA software happens to be a right choice.

The objective of this study is to develop a refined finite element model and a new post processing sub program to determine mixed mode membrane and bending stress intensity factors for arbitrarily located and oriented cracks in a cylindrical shell with tori-spherical end closures subjected to internal pressure loading. To accomplish this objective Finite Element Modelling using ABAQUS, a unified FEA software, and development of a new post processing sub-program 3MBSIF to compute the Stress Intensity Factors Posteriori is presented. The methodology is validated using benchmarks, a set of standard test problems with known target solutions. Selected results of parametric study for arbitrarily oriented cracks of increasing lengths in the toroidal segment are graphically presented and discussed.

1.1 Crack-tip stress field equations and stress intensity factors

Fig. 1 shows the crack-tip coordinate systems(x, y, z) and (r, θ, z) used in stress analysis of cracks. The crack-tip stress field equations in the immediate vicinity of the crack-tip (r<< *a*, where '*a*' denotes crack length) are as follows.

Membrane stress components:

$$\sigma_{xx}(r,\theta,z=0) = \frac{K_I^{(m)}}{\sqrt{2\pi r}} * \cos\frac{\theta}{2}\left[1 - \sin\frac{\theta}{2} * \sin\frac{3\theta}{2}\right] + \frac{K_{II}^{(m)}}{\sqrt{2\pi r}} * \sin\frac{\theta}{2}\left[-2 - \cos\frac{\theta}{2} * \cos\frac{3\theta}{2}\right] \quad (1)$$

$$\sigma_{yy}(r,\theta,z=0) = \frac{K_I^{(m)}}{\sqrt{2\pi r}} * \cos\frac{\theta}{2}\left[1 + \sin\frac{\theta}{2} * \sin\frac{3\theta}{2}\right] + \frac{K_{II}^{(m)}}{\sqrt{2\pi r}} * \sin\frac{\theta}{2} * \cos\frac{\theta}{2} * \cos\frac{3\theta}{2} \quad (2)$$

$$\tau_{xy}(r,\theta,z=0) = \frac{K_I^{(m)}}{\sqrt{2\pi r}} * \sin\frac{\theta}{2} * \cos\frac{\theta}{2} * \cos\frac{3\theta}{2} + \frac{K_{II}^{(m)}}{\sqrt{2\pi r}} * \cos\frac{\theta}{2}\left[1 - \sin\frac{\theta}{2} * \sin\frac{3\theta}{2}\right] \quad (3)$$

Bending stress components:

$$\sigma_{xx}\left(r,\theta,z=\pm\frac{h}{2}\right) = \frac{K_I^{(b)}}{\sqrt{2\pi r}} * \cos\frac{\theta}{2}\left[1 - \sin\frac{\theta}{2} * \sin\frac{3\theta}{2}\right] + \frac{K_{II}^{(b)}}{\sqrt{2\pi r}} * \sin\frac{\theta}{2}\left[-2 - \cos\frac{\theta}{2} * \cos\frac{3\theta}{2}\right] \quad (4)$$

$$\sigma_{yy}\left(r,\theta,z=\pm\frac{h}{2}\right) = \frac{K_I^{(b)}}{\sqrt{2\pi r}} * \cos\frac{\theta}{2}\left[1 + \sin\frac{\theta}{2} * \sin\frac{3\theta}{2}\right] + \frac{K_{II}^{(b)}}{\sqrt{2\pi r}} * \sin\frac{\theta}{2} * \cos\frac{\theta}{2} * \cos\frac{3\theta}{2} \quad (5)$$

$$\tau_{xy}\left(r,\theta,z=\pm\frac{h}{2}\right) = \frac{K_I^{(b)}}{\sqrt{2\pi r}} * \sin\frac{\theta}{2} * \cos\frac{\theta}{2} * \cos\frac{3\theta}{2} + \frac{K_{II}^{(b)}}{\sqrt{2\pi r}} * \cos\frac{\theta}{2}\left[1 - \sin\frac{\theta}{2} * \sin\frac{3\theta}{2}\right] \quad (6)$$

$$\sigma_{zz} = 0 \quad \text{(plane stress assumption)} \quad (7)$$

$$\sigma_{zz} = \nu(\sigma_{xx} + \sigma_{yy}) \text{ (plane strain assumption)} \quad (8)$$

The stresses in the immediate vicinity of the crack-tip $\left(\frac{r}{a} \ll 1\right)$ are singular. It can be seen from the above equations that both membrane stresses (mid-surface) and bending stresses (top and bottom surface) have the same inverse square root singularity and the same distribution with respect to θ as in the case of pure stretching [2] and bending [3].

It is also seen that the distribution of singular stresses with respect to (r,θ) is independent of the shell wall thickness. However, in the solution of any specific problem, the thickness effect will be seen in the values of the stress intensity factors denoted by $K_I^{(m)}, K_{II}^{(m)}, K_I^{(b)}$ and $K_{II}^{(b)}$. These stress intensity factors are formally defined as the rate at which the stress components

σ_{yy} and τ_{xy} approach infinity at the crack-tip (r = 0) in the plane of the crack $(\theta = 0)$:

$$K_I^{(m)} = \lim_{\delta^+\to 0}\sqrt{2\pi\delta} * \sigma_{yy}(r=\delta, \theta=0, z=0) \quad (9)$$

$$K_{II}^{(m)} = \lim_{\delta^+\to 0}\sqrt{2\pi\delta} * \tau_{xy}(r=\delta, \theta=0, z=0) \quad (10)$$

$$K_I^{(b)} = \lim_{\delta^+\to 0}\sqrt{2\pi\delta} * \sigma_{yy}\left(r=\delta, \theta=0, z=\pm\frac{h}{2}\right) \quad (11)$$

$$K_{II}^{(b)} = \lim_{\delta^+\to 0}\sqrt{2\pi\delta} * \tau_{xy}\left(r=\delta, \theta=0, z=\pm\frac{h}{2}\right) \quad (12)$$

Specifically, $K_I^{(m)}$ is the mode I membrane stress intensity factor, $K_{II}^{(m)}$ is the mode II membrane stress intensity factor, $K_I^{(b)}$ is the mode I bending stress intensity factor, and $K_{II}^{(b)}$ is the mode II bending stress intensity factor. These Stress Intensity Factors completely characterize the near crack-tip stress fields. They are a function of shell geometry, wall thickness, crack length, crack location and orientation, applied loads and boundary conditions.

II. FINITE ELEMENT MODELLING

Finite Element Modelling is defined here as the analyst's choice of material models, finite elements, meshes, constraint equations, analysis procedures, governing matrix equations and their solution methods, specific pre- and post-processing options available in a chosen commercial FEA software for determination of mixed mode membrane and bending stress intensity factors for shell structures with arbitrarily located and oriented cracks under different types of applied loads and boundary conditions.

In this study, ABAQUS is used for FE Modelling. A fine mesh of singular isoparametric curved shell elements (STRIA6), triangular in shape and quadratic in order with six nodes and six engineering degrees of freedom at each node with user specified number *NS* from one crack face to another and size Δa is created around each crack-tip. The rest of the domain under consideration is discretized using a compatible mesh of 8-noded curved shell element, quadrilateral in shape and quadratic in order (QUAD8) and 6-noded curved shell element of triangular shape (TRIA6). A brief description of these elements is given below.

The QUAD8 element is shown in figure 2. The TOP, BOTTOM and MIDDLE surfaces of the element are curved, whereas the sections across the thickness are generated by the straight lines. The geometric modelling requires specification of two vectors at each of the eight mid surface nodes. One is the position vector R_i of the node i, with the three global Cartesian components X_i, Y_i, Z_i, where the subscript i identifies the node number. The other is the unit normal vector V_3^i along with the wall thickness t_i of the same nodes. The QUAD8 element carries six engineering degrees of freedom $(U_i, V_i, W_i, \theta_{Xi}, \theta_{Yi}, \theta_{Zi})$ at each of the eight mid surface nodes. The nodal degrees of freedom are illustrated in Fig. 2. Further details are available in ABAQUS software documentation.

The TRIA6 element shown in fig. 3 has six nodes and six engineering degrees of freedom at each node. The matrices and vectors for this element are computed as follows: The edge 1-4-8 of the QUAD8 element is collapsed and nodes 4 and 8 are co-located with node 1. Nodes 1, 4 and 8 are tied together to have the same degrees of freedom using multipoint constraint equations.

The Singular Isoparametric Triangular Shell element (STRIA6), shown in fig. 4, has six nodes and six engineering degrees of freedom at each node. The matrices and vectors for this element are computed as follows: The nodes 4 and 6 which are normally located at mid side positions in the TRIA6 element are moved to the quarter point locations close to node 1. Node 1 in turn is located at a crack-tip. An analysis of the displacement, Strain and Stress field at any point within this element shows that the membrane and bending stress components exhibit the well known $1/\sqrt{r}$ singularity. The number of STRIA6 elements used around a crack-tip can be progressively increased and their length reduced till accurate stress intensity factor solution is achieved. This demands a specific pre-processing capability. The pre-processing capability in ABAQUS enables the creation of progressively refined mesh of STRIA6 element around each crack-tip with user specified NS and Δa. A compatible mesh of regular elements (QUAD8 and TRIA6) then completes the FE Model.

Consistent with this FE Model, the stress intensity factors have to be calculated posteriori. A critical assessment of post-processing options for Computational Fracture Mechanics in ABAQUS identified the need for development and validation of a special purpose post-processing sub-program for computation of mixed mode membrane and bending stress intensity factors. This program is called 3MBSIF and an overview of this is given in next section.

III. POST PROCESSING SUB PROGRAM – 3MBSIF

A Post Processing sub program 3MBSIF to calculate posteriori Stress Intensity Factors $K_I^{(m)}$, $K_{II}^{(m)}$, $K_I^{(b)}$, and $K_{II}^{(b)}$ and out put their normalised values is developed in this study. The Stress Intensity Factors are computed using the nodal degrees of freedom of flagged nodes located on flagged singular elements at a crack-tip. Fig. 5 shows a typical mesh of STRIA6 elements around a crack-tip. There is a need to define a local Cartesian coordinate system (x, y, z) at a crack-tip and automate the computation of their direction cosines. These are used to create a Transformation matrix $[\lambda]$.

$$[\lambda] = \begin{bmatrix} \cos(x,X) & \cos(x,Y) & \cos(x,Z) \\ \cos(y,X) & \cos(y,Y) & \cos(y,Z) \\ \cos(z,X) & \cos(z,Y) & \cos(z,Z) \end{bmatrix} \quad (13)$$

where, X, Y, Z denote global Cartesian coordinate system used in the solver.

The nodal degrees of freedom in the crack-tip Cartesian coordinate system (x, y, z) are then computed as

$$\begin{bmatrix} u_i \\ v_i \\ w_i \end{bmatrix} = [\lambda] \begin{bmatrix} U_i \\ V_i \\ W_i \end{bmatrix} \quad (14)$$

$$\begin{bmatrix} \theta_{xi} \\ \theta_{yi} \\ \theta_{zi} \end{bmatrix} = [\lambda] \begin{bmatrix} \theta_{Xi} \\ \theta_{Yi} \\ \theta_{Zi} \end{bmatrix} \quad (15)$$

Consistent with the use of STRIA6 element, the membrane stress intensity factors are calculated using the following formulae.

$$K_I^{(m)} = \frac{E}{(1+\nu)(\chi+1)} \left(\frac{\pi}{2\Delta a}\right)^{\frac{1}{2}} \left[4\left(\bar{v}_l - \bar{v}_{l'}\right) - \left(\bar{v}_m - \bar{v}_{m'}\right)\right] \quad (16)$$

$$K_{II}^{(m)} = \frac{E}{(1+\nu)(\chi+1)} \left(\frac{\pi}{2\Delta a}\right)^{\frac{1}{2}} \left[4\left(\bar{u}_l - \bar{u}_{l'}\right) - \left(\bar{u}_m - \bar{u}_{m'}\right)\right] \quad (17)$$

where,

E is the Young's modulus, ν is the Poisson's ratio, $\chi = \frac{(3-\nu)}{(1+\nu)}$ (plane stress assumption), and $\chi = (3 - 4\nu)$ (plane strain assumption), $\bar{u}_l, \bar{u}_m, \bar{v}_l, \bar{v}_m, \bar{u}_{l'}, \bar{u}_{m'}, \bar{v}_{l'}, \bar{v}_{m'}$ are the relative nodal displacement at nodes l, l', m, m' with reference to the crack-tip node i.

The bending stress intensity factors are calculated using the following formulae

$$K_I^{(b)} = \frac{E}{(1+\nu)(\chi+1)} \left(\frac{\pi}{2\Delta a}\right)^{\frac{1}{2}} \left[4 \cdot \frac{h}{2}\left(\sin \bar{\theta}_x^l - \sin \bar{\theta}_x^{l'}\right) - \frac{h}{2}\left(\sin \bar{\theta}_x^m - \sin \bar{\theta}_x^{m'}\right)\right] \quad (18)$$

$$K_{II}^{(b)} = \frac{E}{(1+\nu)(\chi+1)} \left(\frac{\pi}{2\Delta a}\right)^{\frac{1}{2}} \left[4 \cdot \frac{h}{2}\left(\sin \bar{\theta}_y^l - \sin \bar{\theta}_y^{l'}\right) - \frac{h}{2}\left(\sin \bar{\theta}_y^m - \sin \bar{\theta}_y^{m'}\right)\right] \quad (19)$$

where,

$\bar{\theta}_x^l = (\theta_x^l - \theta_x^i)$, $\bar{\theta}_y^l = (\theta_y^l - \theta_y^i)$, etc., and h denotes the thickness at crack-tip node i.

It is important to note the use of $\sin \theta_x, \sin \theta_y$ instead of θ_x and θ_y.

In 3MBSIF, a local Cartesian coordinate system (x, y, z) is created at each crack-tip as illustrated in fig. 5. The direction cosines of x, y, z-axis are computed using the global Cartesian coordinates of node i (at crack-tip), node j and node k as identified in fig. 5. These direction cosines are used to construct the Transformation matrix $[\lambda]$.

The nodal degrees of freedom, at nodes i (crack-tip), l, l', m, m' identified in fig. 5 with respect to the Global Cartesian coordinate (X, Y, Z), are extracted from the solver output and transformed to the crack-tip coordinate

system (x, y, z). The transformed nodal degrees of freedom are then used to calculate Stress Intensity Factors $K_I^{(m)}, K_{II}^{(m)}, K_I^{(b)}$ and $K_{II}^{(b)}$ using formulae presented earlier.

The Stress Intensity Factors are normalised using $K_0 = \sigma_0\sqrt{\pi a}$, where, σ_0 is a reference stress input by the user and a is the crack length.

IV. BENCHMARKS

A benchmark is a standard test problem with known target solution in the form of Formulae/Graphs/Tables. These are used to validate finite element models developed using ABAQUS and stress intensity factors calculated using 3MBSIF.

4.1 Test Problem 1

A cylindrical shell of radius R, length $2L$, Wall thickness t, with an axially oriented crack of length $2a$, is subjected to internal pressure p. $R = 1000\ mm$, $L = 1000\ mm$, $t = 10\ mm$, $p = 1\ MPa$, $E = 2 \times 10^5\ N/mm^2$, and $v = 0.3$ are used in the computation.

The target solution taken from Murthy [4] is presented in Fig. 6. It is to be noted that the crack length parameter is given by

$$\beta^2 = \frac{a^2}{8Rt}[12(1 - v^2)]^{\frac{1}{2}} \qquad (20)$$

A refined finite element mesh of STRIA6 elements with $NS = 36$ and $\Delta a = a/100$ at each crack-tip and a compatible mesh of QUAD8 and TRIA6 elements in the rest of the domain was created and a linear static analysis was performed using ABAQUS. Extracting the nodal degrees of freedom at flagged nodes on flagged singular elements, the stress intensity factors K_I^m and K_I^b are calculated using 3MBSIF. They are normalised using $K_0 = \sigma_0\sqrt{\pi a}$, with $\sigma_0 = pR/t$. The computed results are presented in Table 1.

Overall the comparison indicated very good agreement for K_I^m. The difference in K_I^b is attributed to the Shear Deformation Theory used in the present analysis. The target solution is based on classical shallow thin shell theory.

4.2 Test Problem 2

A cylindrical shell of radius R, length L, Wall thickness t, with a circumferentially oriented crack of length $2a$, is subjected to axial force P. $R = 1000\ mm$, $L = 1000\ mm$, $t = 10\ mm$, $P = 1\ kN$, $E = 2 \times 10^5$ N/mm² and $v = 0.3$ are used in the computation. The target solution taken from Murthy[4] is presented in Fig. 7.

A refined mesh of STRIA6 elements with $NS = 36$ and $\Delta a = a/100$ at each crack-tip and a compatible mesh of regular elements QUAD8 and TRIA6 elements in the rest of the domain was created and a linear static analysis was performed using ABAQUS. Stress intensity factors K_I^m and K_I^b are posteriori calculated using 3MBSIF. They are

normalised using $K_0 = \sigma_0\sqrt{\pi a}$, where $\sigma_0 = P/2\pi R t$. The computed results are presented in Table 2.

Overall the comparison between the present finite element solution and the target results based on continuum mechanics method is very good for $\beta < 1.5$. For larger values of β, the notable significant difference is attributed to severe local bulging observed during graphical post processing of the results around each crack-tip.

4.3 Test Problem 3

A Spherical shell of radius R, wall thickness t, with a meridional crack of length $2a$, is subjected to internal pressure p. Computations are performed with $R = 500\ mm$, $t = 5\ mm$, $p = 1\ MPa$, $E = 2 \times 10^5\ GPa$, $v = 0.3$ and $a = 0.5, 15\ and\ 50\ mm$.

Target solution taken from Murakami [5] is for mode I membrane stress intensity factor denoted by K_t:

$K_t = \sigma_0\sqrt{\pi a} * F(\lambda)$, where the reference stress $\sigma_0 = \frac{pR}{2t}$, Crack length parameter $\lambda = \frac{a}{\sqrt{Rt}}$, and $F(\lambda) = \sqrt{(1 + 1.41\lambda^2 + 0.04\lambda^3)}$

Exploiting symmetry, one quarter of the spherical shell was discretised. A fine mesh of STRIA6 element with $NS = 36$ and $\Delta a = a/100$ was used around the crack-tip as illustrated in fig. 8. The rest of the domain is discretised using QUAD8 and TRIA6 elements. Symmetry conditions enforced are also shown in fig. 8. A consistent calculation of nodal forces due to applied internal pressure is included. A linear static analysis was performed and the crack-tip stress intensity factors were calculated posteriori using 3MBSIF.

The calculated Stress intensity factor K_t is presented in Table 3 along with the target solution. For a very small crack the difference between the two solutions is negligible. However, for longer cracks, there is a growing difference between the two solutions. The target solution is acceptable for $\lambda \leq 0.3$. For larger values of λ the present solution is believed to be accurate.

V. CASE STUDY

The geometric model of a long cylindrical shell with tori-spherical end closures is shown in fig. 9. One octant of this model with a crack oriented at an angle $\alpha = 45°$ with respect to the circumferential direction in the toriodal segment is presented in fig. 10. Finite element modelling for a circumferentially oriented crack ($\alpha = 0°$) along with symmetric boundary conditions is presented in fig. 11. A refined mesh of singular elements (STRIA6) with a compatible mesh of regular elements (QUAD8 and TRIA6) used in the present study is illustrated in fig. 12. A consistent calculation of nodal forces due to the applied internal pressure loading is included in the analysis.

The geometric dimensions used in the computation are: radius of cylindrical segment R =120 mm, Radius of the

spherical segment $R_s = 240\ mm$, Radius of toroidal segment $R_t = 20\ mm$, Thickness of the shell (t) = 1.2 mm. The applied internal pressure p = 1MPa. The material properties are $E = 2 \times 10^5\ N/mm^2$ and $v = 0.3$. The graphical post processing capability in ABAQUS is demonstrated in fig.s 13-15, where line contour plots of von Mises equivalent stress around a crack-tip are displayed. The software permits such plots to be displayed at top, mid and bottom surfaces of the shell. Knowing the yield strength of the material it is then possible to map the elastic plastic boundary and study the variation of crack-tip plastic zone shape and size along the crack front. A linear static analysis provided the necessary inputs to capture these results.

Using the standard output files of a linear static analysis of the finite element model the necessary input for the Special purpose post processing sub-Program 3MBSIF is extracted and the crack-tip stress intensity factors are computed. Results of a parametric study where the crack length parameter β is varied from 0 to 1.6 and the orientation angle α is varied from $0°$ to $90°$ are presented in tables 4 to 7 for future reference. These results are believed to be converged and hence accurate to be used as target solution in future investigations.

The significance of using plane stress or plane strain assumption in computing the stress intensity factors $K_I^{(m)}$, $K_{II}^{(m)}$, $K_I^{(b)}$ and $K_{II}^{(b)}$ is clear from these tables. The range of β covered is to restrict the crack to the toroidal segment. Larger values would make the crack-tips to penetrate the cylindrical and spherical segments. It is interesting to note that even for symmetric orientations of the crack namely circumferential $(\alpha = 0°)$ and meridional $(\alpha = 90°)$ both mode I and mode II components of membrane and bending stress intensity factors are significant. The fracture therefore is of mixed mode type and demands an investigation in to its prediction and verification.

A graphical presentation of these results is made in fig.s 16 to 19. The variations of stress intensity factors $K_I^{(m)}$, $K_{II}^{(m)}$, $K_I^{(b)}$ and $K_{II}^{(b)}$ with respect to α and β are quite smooth. The magnitudes of bending stress intensity factors are small in comparison with the membrane stress intensity factors. However the results presented are for thin walled shells with radius to thickness ratio of 100. It is anticipated that for thicker shells with radius to thickness ratio between 10 and 100 the bending stress intensity factors become significant. For larger values of crack length parameter β, it is anticipated that the junction stresses between the cylindrical and toriodal segments and between the toroidal and spherical segments will significantly influence the stress intensity factors. The coupled effect of thickness ratio and junction stresses deserves an in depth study. It is gratifying to note that the proposed finite element model and the developed post processing sub program are capable of handling this problem.

VI. CLOSURE

Determination of mixed mode membrane and bending stress intensity factors for arbitrarily located and oriented cracks in complex shell structures is a challenging task. A unified approach to this problem appears to be finite element modelling using commercial FEA software. Specifically a progressively refined mesh of singular isoparametric triangular shell element (STRIA6) is used around each crack-tip. A compatible mesh of quadratic isoparametric quadrilateral shell element (QUAD8) and quadratic isoparametric triangular shell element (TRIA6) is used to discretise rest of the domain. However, the crack-tip stress intensity factors have to be calculated posteriori. The chosen commercial FEA software should therefore have the required pre-processing and post processing capabilities.

In the present study, ABAQUS, a unified FEA software is chosen. It has the required pre-processing capabilities for finite element modelling of cracked shell structures as demonstrated in this paper. However there was a need to develop, validate and use a special purpose post processing sub-program to calculate the mixed mode membrane and bending stress intensity factors at each crack-tip. The end product is a validated finite element model and a new post processing sub-program 3MBSIF that provided accurate stress intensity factors for the problem of a pressurised cylindrical shell with torispherical end closures with arbitrarily oriented cracks in the cylindrical, spherical and toroidal segments.

The presented stress intensity factors are essential to predict (1) Mixed mode fracture under static, dynamic and sustained loads (2) Residual strength and (3) Crack growth life under cyclic loading conditions. However there is a clear need to verify the predictions using experimental investigations

REFERENCES

1. Raju I.S. and Newman J.C., Methods for analysis of crack problems in three dimensions", *Journal of Aeronautical Society of. India*, Special issue on fracture mechanics, Part I, 36 (3) 1984.

2. Williams M. L. On the Stress Distribution at the Base of a Stationary crack, *ASME Trans. Journal of Applied Mechanics*, 24, 1957, 109-114

3. Murthy, M. V. V., K. N. Raju and S. Viswanath (), On the Bending Stress Distribution at the tip of a Stationary Crack from Reissner's Theory, *International Journal of Fracture*, 17(6), 1981, 537-552

4. Murthy, M. V. V., Rao, K. P. and Rao A. K., On the Stress Problem of Large Elliptical cut outs and cracks in circular cylindrical Shells, *International Journal of Solids and Structures*, 10, 1974, 1243-1269.

5. Murakami et al. (Editors) (1987), *Stress Intensity factors handbook, Vols. 1 and 2*, Pergamon Press, Oxford
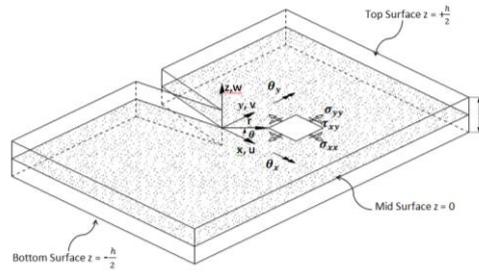
Figure 1: Crack-tip coordinate systems and stress components
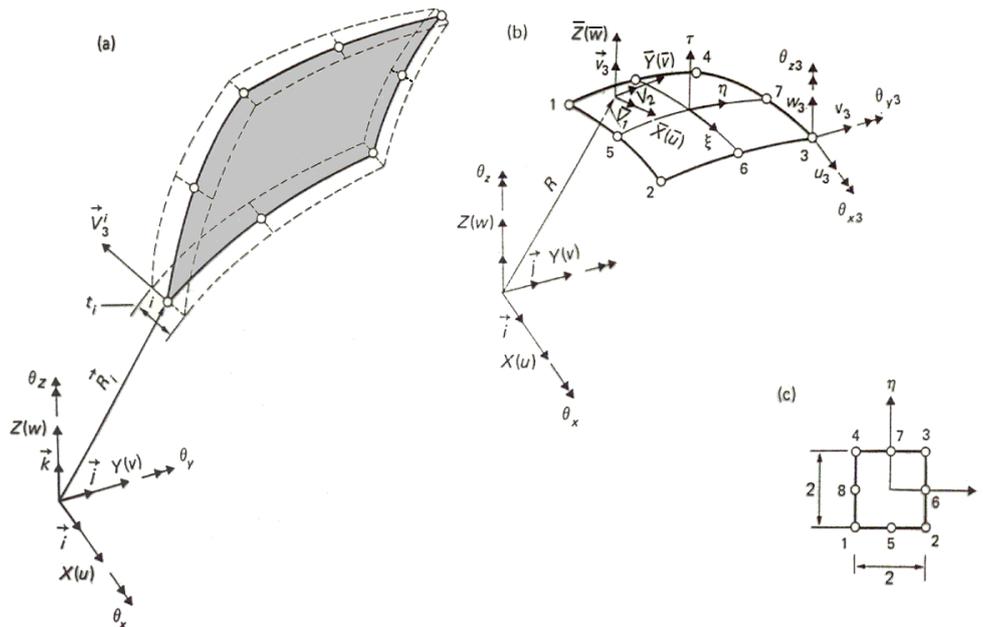
Figure 2. Curved Isoparametric Shell Element of Quadrilateral Shape (QUAD 8)
(a) Element Geometry (b) Coordinate System and Nodal Degrees of Freedom (c) Parent Element and Node Numbering System
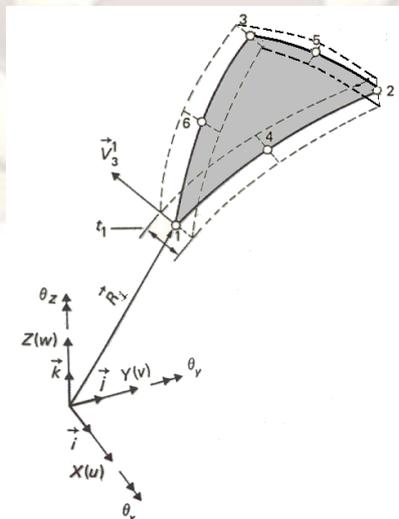
Figure 3. Curved Isoparametric Shell Element of Triangular Shape (TRIA 6)
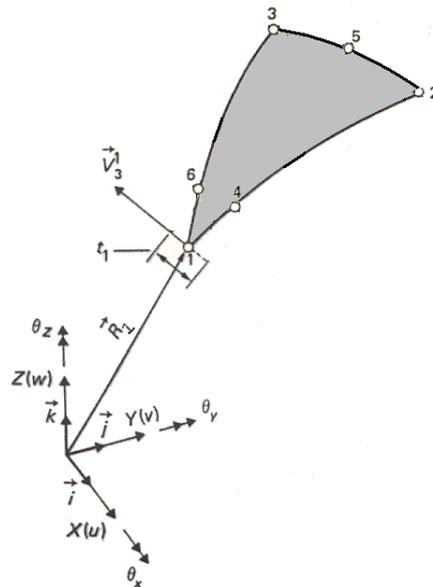
Figure 4. Singular Isoparametric Shell Element Of Triangular Shape (STRIA 6)
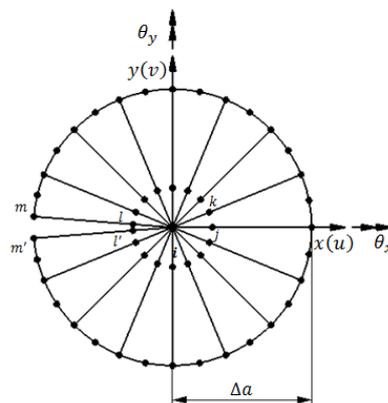
Figure 5. Singular element mesh around a crack-tip and local Cartesian coordinates
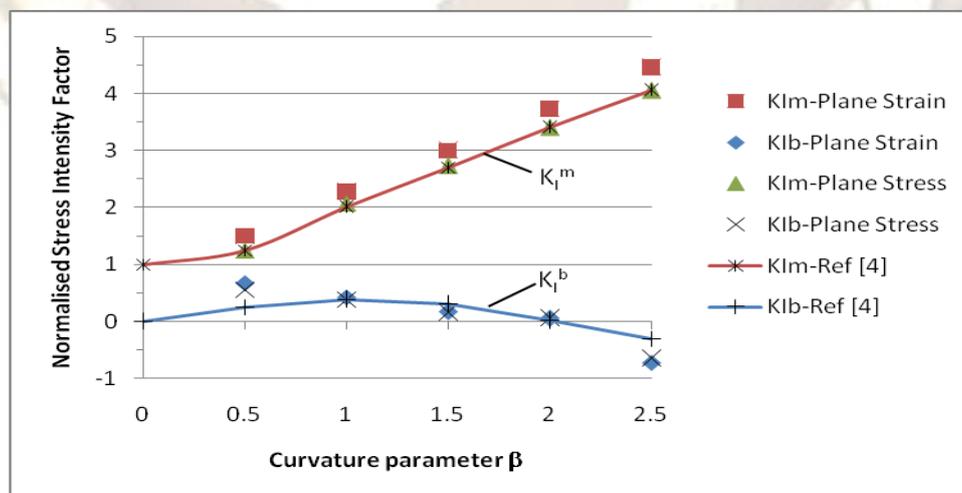
Figure 6. Membrane and bending stress intensity factors for an axially located crack in a cylindrical shell under internal pressure
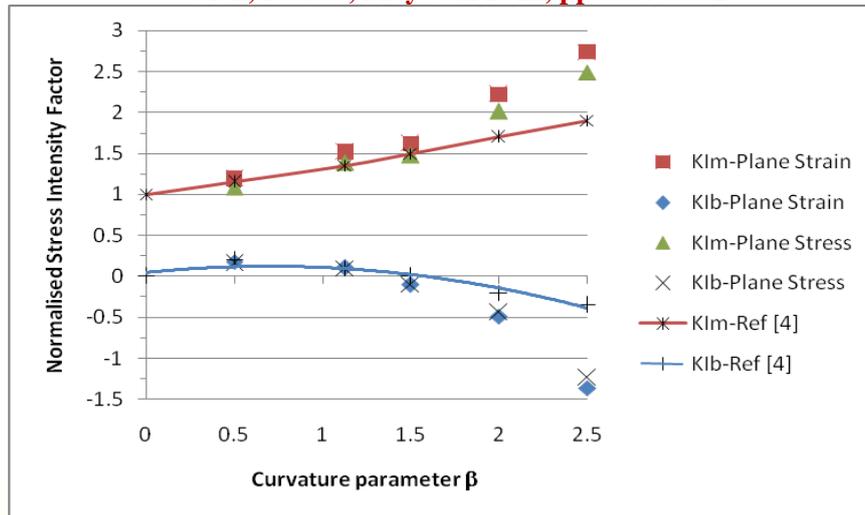
Figure 7. Membrane and bending stress intensity factors for circumferentially oriented crack in a cylindrical shell under axial force.
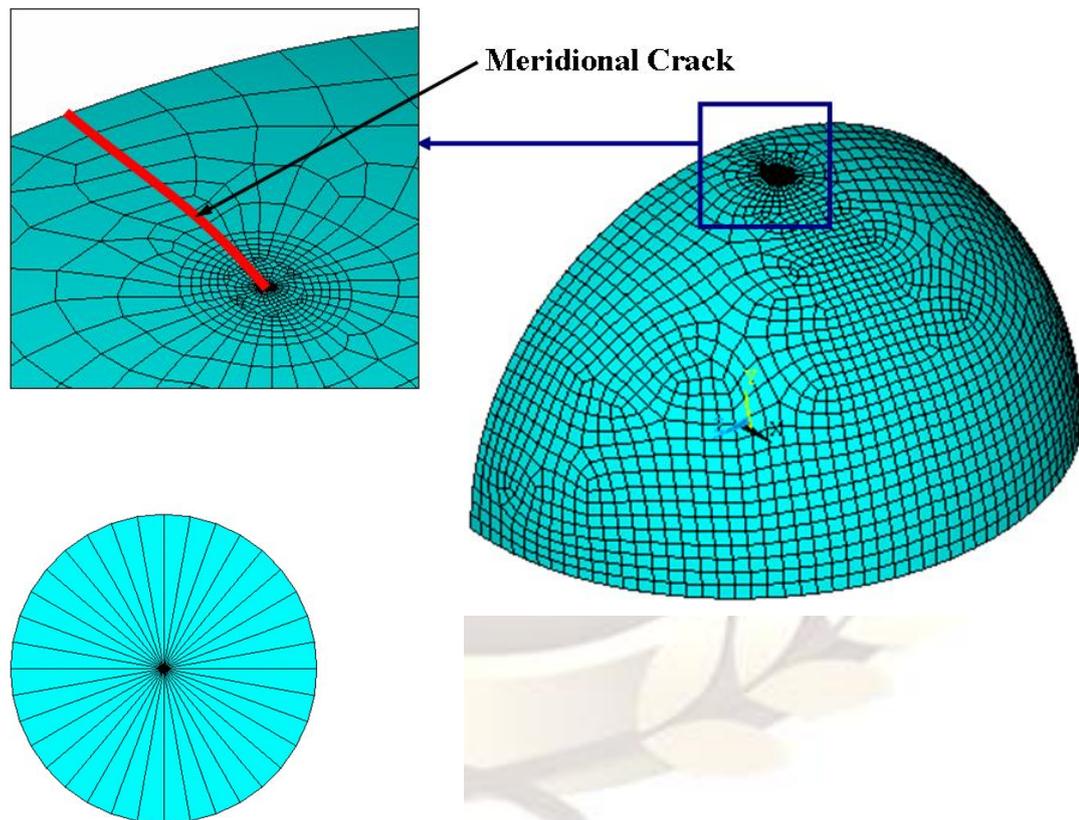
Figure 8. Finite Element Model of a spherical shell with a Meridional crack
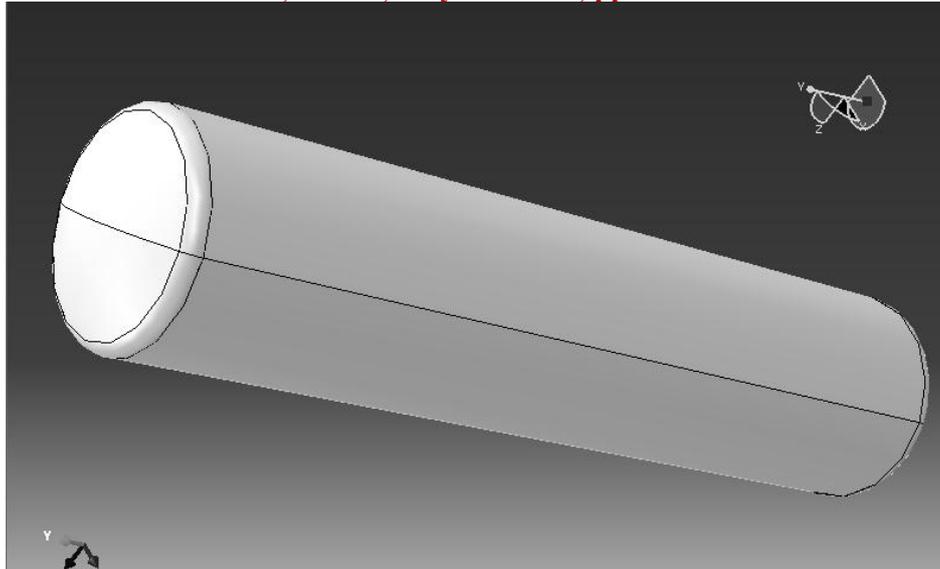
Figure 9. Geometric model of a Cylindrical Shell with Tori-Spherical End Closures
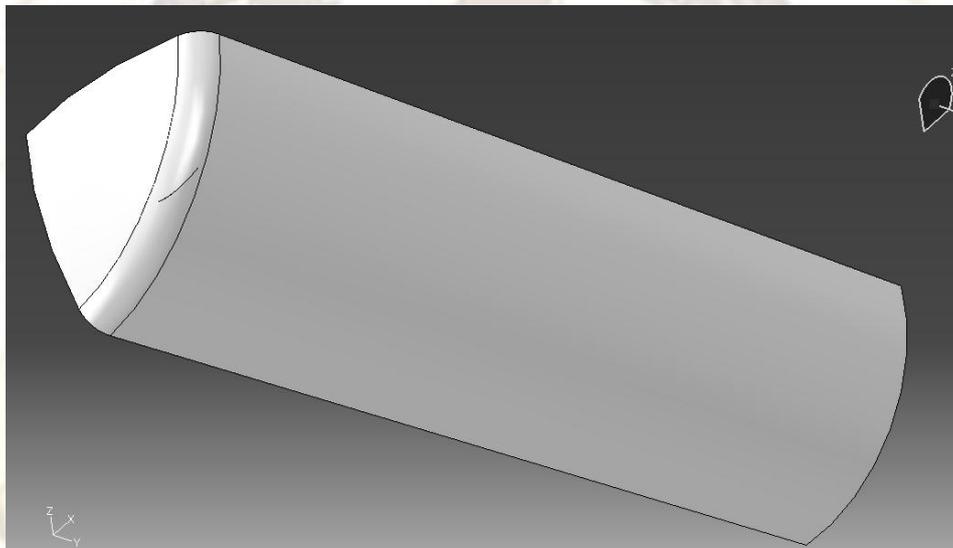
Figure 10. Cylindrical Shell with Tori-Spherical End Closures with 45º oriented crack in the Toroidal Segment.
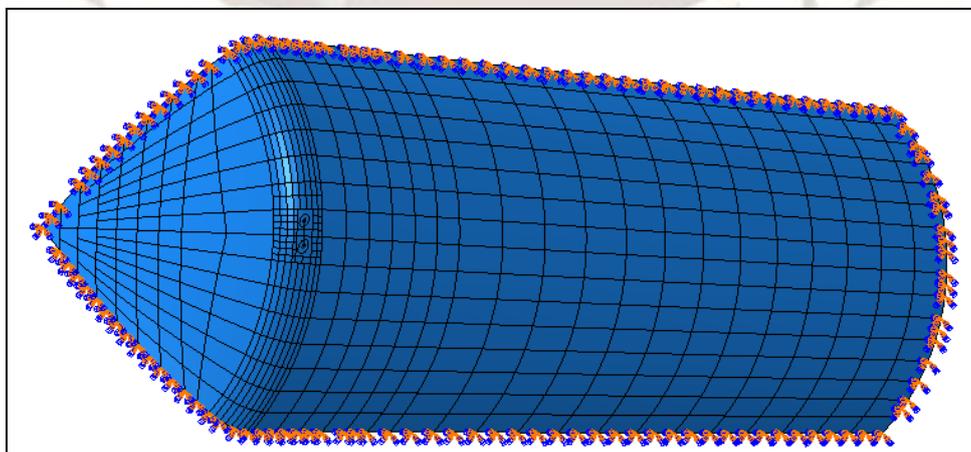
Figure 11. Cylindrical Shell with Tori-Spherical End Closures; FE model for Circumferential Crack
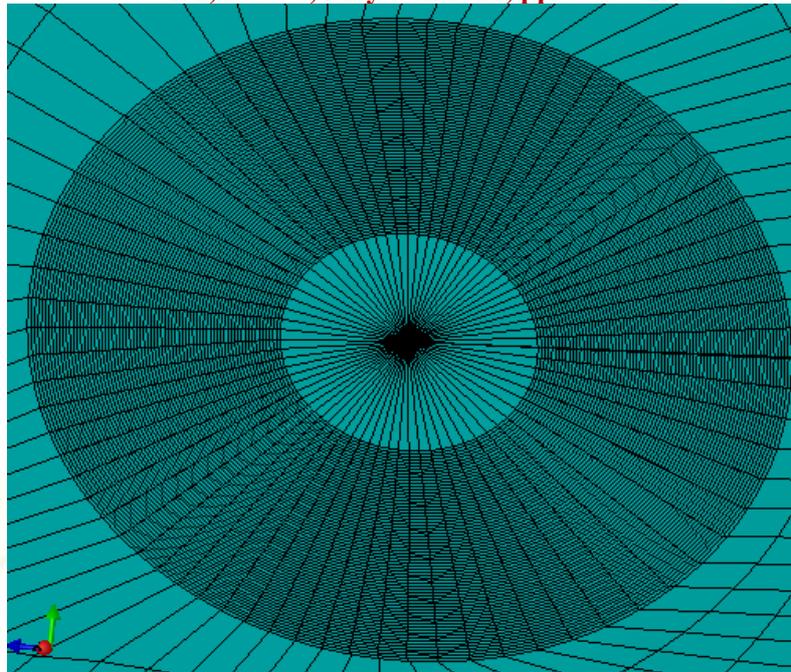
Figure 12. Cylindrical Shell with Tori-Spherical End Closures; Singular Element Mesh (NS = 72, Δa = a/100) around the Crack tip.
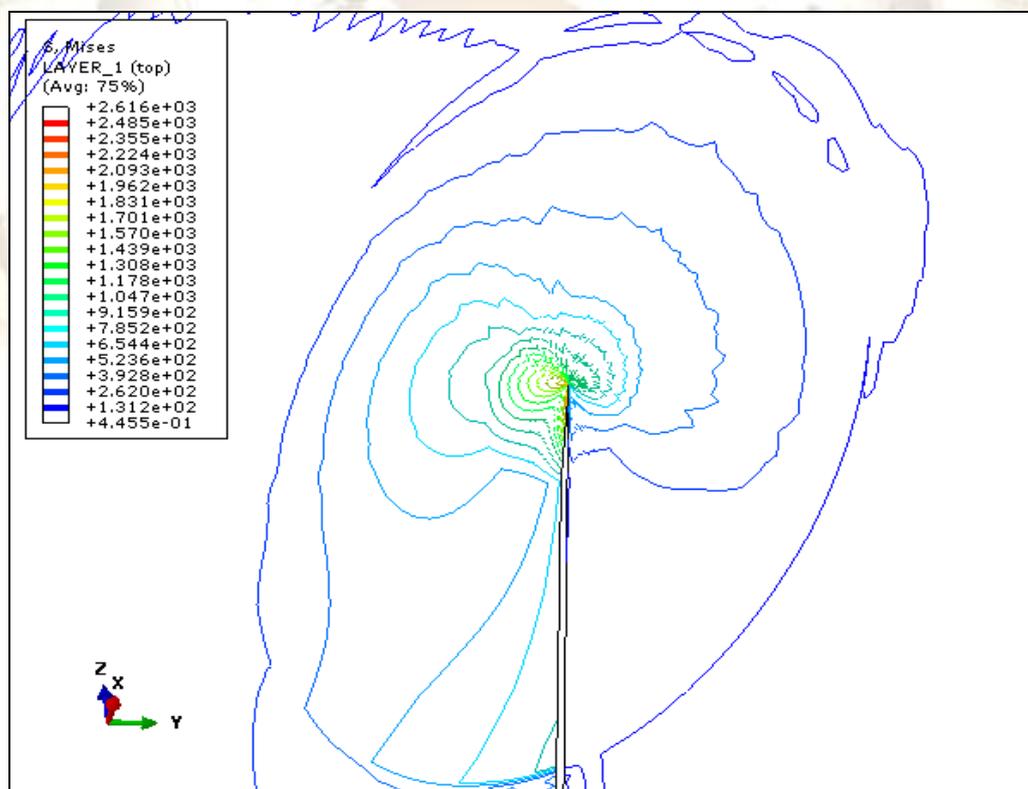
Figure 13. Cylindrical Shell with Tori-Spherical End Closures;von Mises Stress Contours around a Crack Tip (Circumferential Crack, α = 0º, β =1.0, (R/h) =100, at Top Surface)
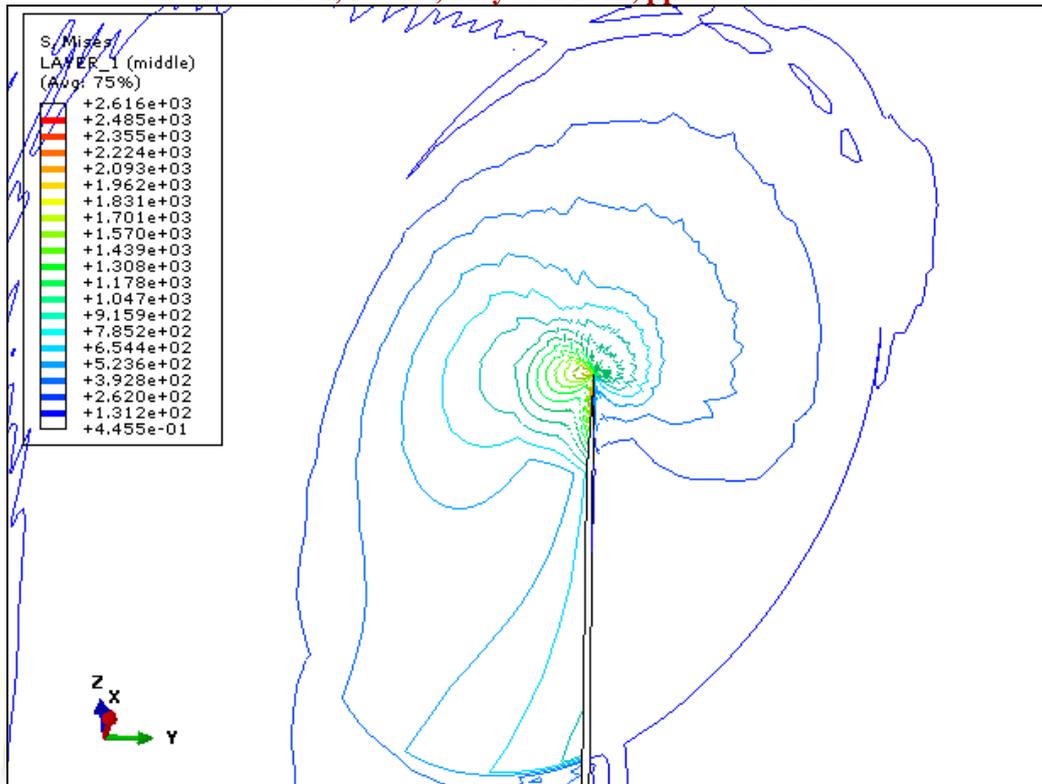
Figure 14. Cylindrical Shell with Tori-Spherical End Closures;von Mises Stress Contours around a Crack Tip (Circumferential Crack, α = 0º, β =1.0, (R/h) =100, At Middle Surface)
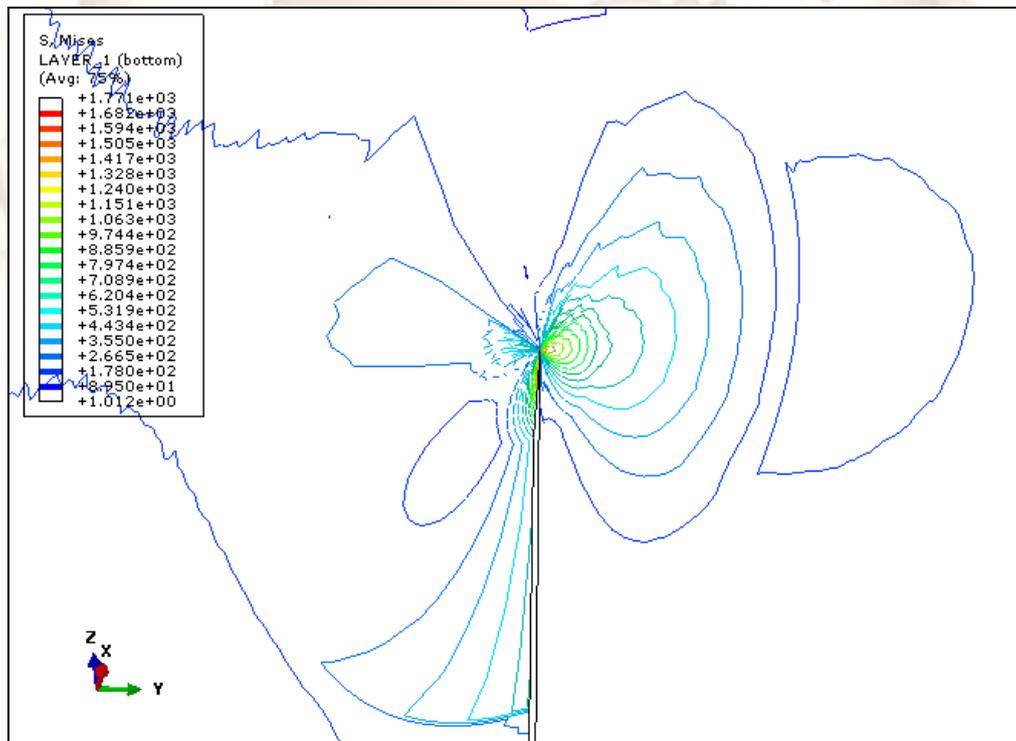
Figure 15. Cylindrical Shell with Tori-Spherical End Closures; von Mises Stress Contours around a Crack Tip (Circumferential Crack, α = 0º, β = 1.0, (R/h) = 100, At Bottom Surface)
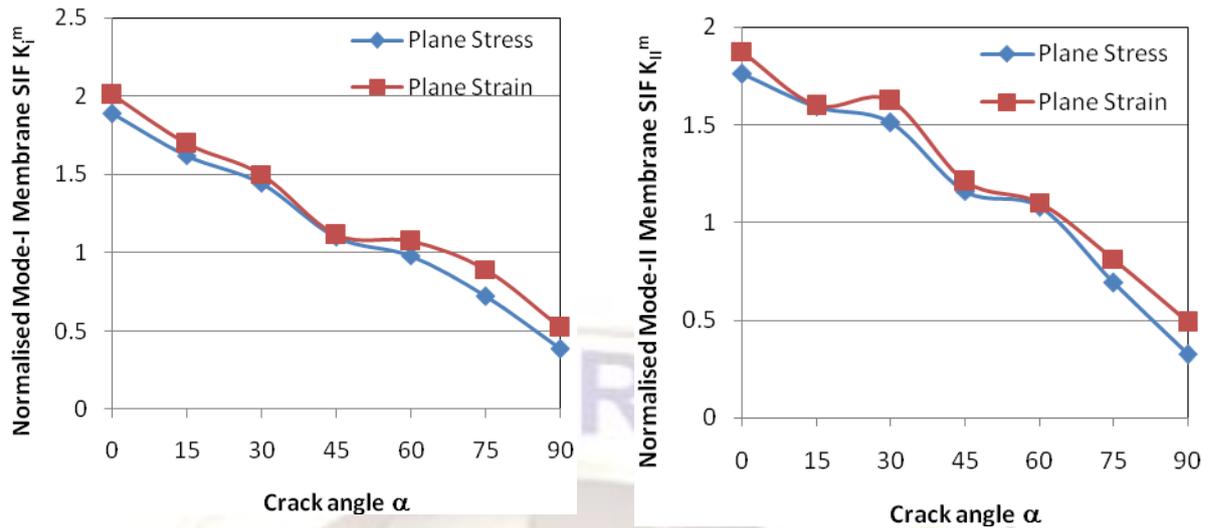
Figure 16. Variation of Mode I and Mode II Membrane SIF with α (β = 1.0, (R/h) = 100)
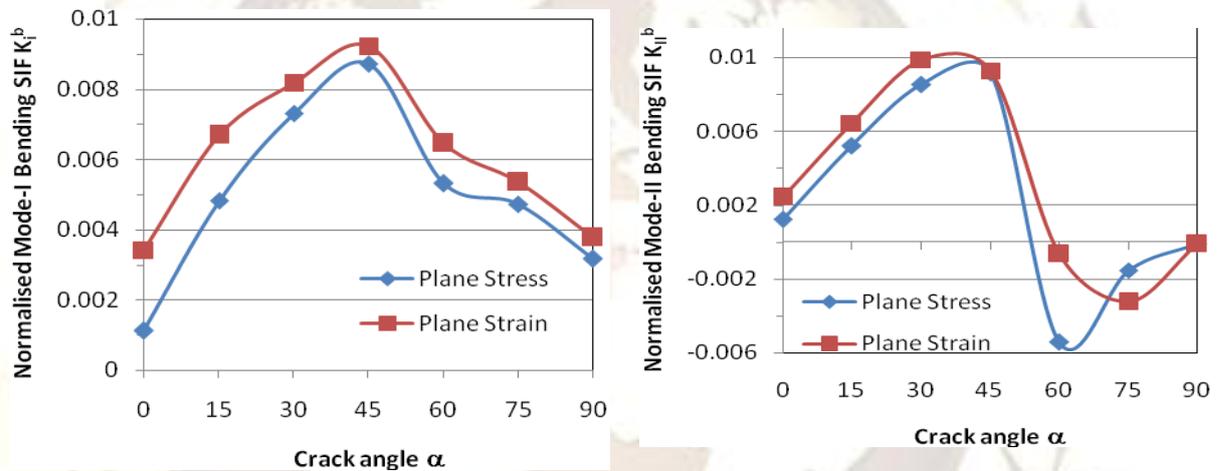
Figure 17. Variation of Mode I and Mode II Bending SIF with α (β = 1.0, R/h = 100)
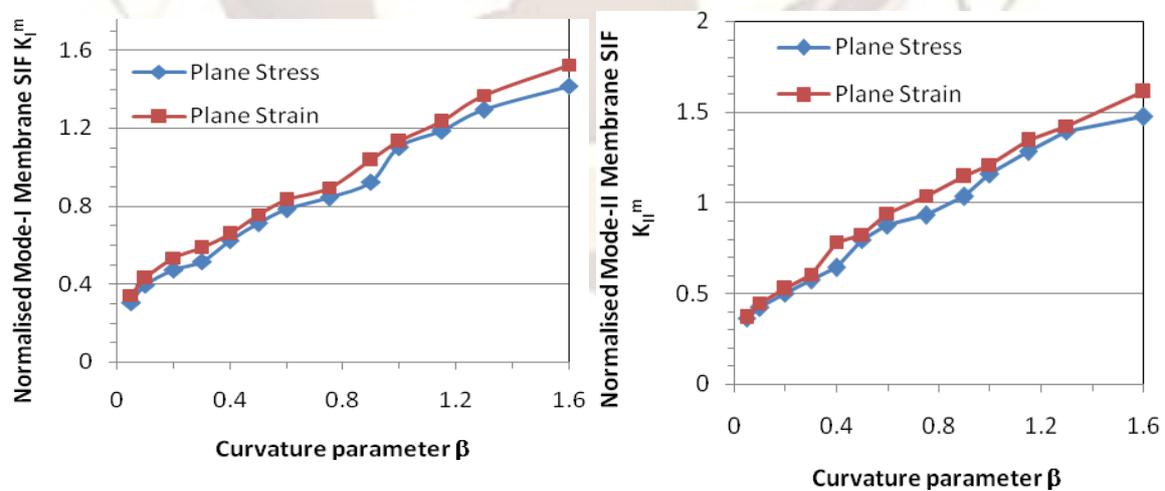
Figure 18. Variation of Mode I and Mode II Membrane SIF with β (α = 45°, (R/h) =100).
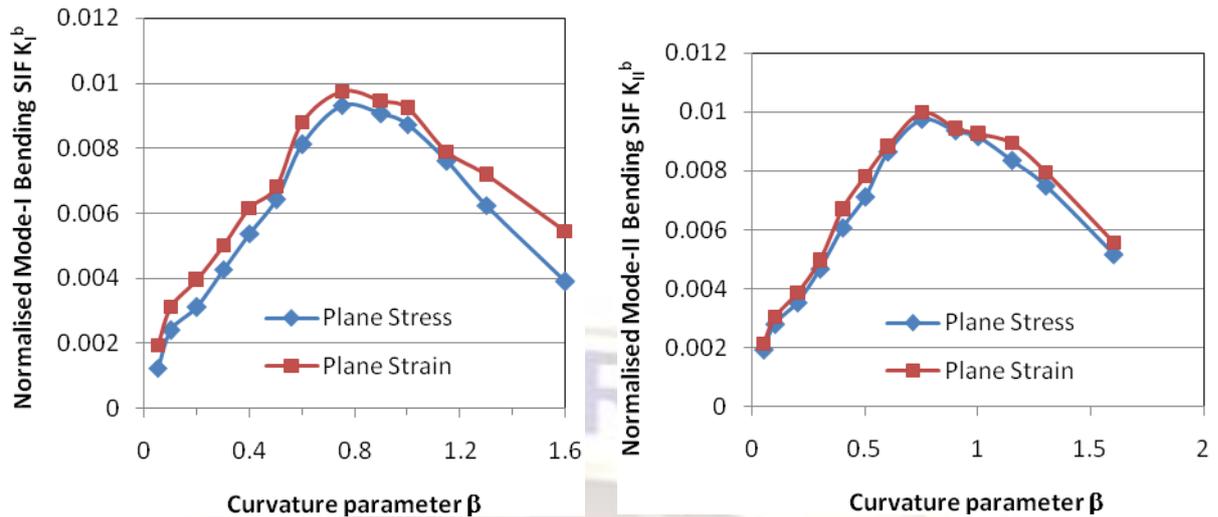
Figure.19. Variation of Mode I and Mode II Bending SIF with β (α = 45°, (R/h) =100).

Table 1. Membrane and bending stress intensity factors for axially oriented crack in a cylindrical shell subjected to internal pressure

β	Plane strain assumption		Plane stress assumption		Target [4]	
	K_I^m (Normalized)	K_I^b (Normalized)	K_I^m (Normalized)	K_I^b (Normalized)	K_I^m (Normalized)	K_I^b (Normalized)
0.5	1.4981	0.6755	1.245	0.5617	1.25	0.25
1.0	2.2723	0.4275	2.067	0.389	2.0	0.38
1.5	2.9964	0.1617	2.7267	0.1471	2.7	0.3
2.0	3.733	0.05145	3.397	0.04682	3.4	0.01
2.5	4.4547	-0.7267	4.0538	-0.6613	4.05	-0.3

Table 2. Membrane and bending stress intensity factors for circumferentially oriented crack in a cylindrical shell under axial force.

β	Plane strain assumption		Plane stress assumption		Target [4]	
	K_I^m (Normalized)	K_I^b (Normalized)	K_I^m (Normalized)	K_I^b (Normalized)	K_I^m (Normalized)	K_I^b (Normalized)
0.5	1.19	0.18	1.084	0.162	1.15	0.2
1.13	1.52	0.111	1.383	0.101	1.35	0.1
1.5	1.62	-0.104	1.48	-0.095	1.5	0.0
2.0	2.22	-0.487	2.017	-0.443	1.7	-0.2
2.5	2.74	-1.36	2.49	-1.24	1.9	-0.35

Table 3. Stress intensity factor K_t for a pressurized spherical shell with a meridional crack

λ	Present study	Target [5]	% difference
0.01	62.73	62.67	0.09
0.3	392.07	364.54	1.02
1.0	1174.21	980.87	16.47

Table 4. Membrane Stress Intensity Factors for β = 1 and α = 0º to 90º

Crack Angle α	Plane Stress Assumption		Plane Strain Assumption	
	$K_I^{(m)}$	$K_{II}^{(m)}$	$K_I^{(m)}$	$K_{II}^{(m)}$
0º	1.89	1.762	2.01	1.874
15º	1.621	1.594	1.694	1.598
30º	1.443	1.513	1.502	1.622
45º	1.102	1.16	1.113	1.211
60º	0.9812	1.08	1.072	1.101
75º	0.723	0.693	0.894	0.812
90º	0.387	0.326	0.521	0.489

Table 5. Bending Stress Intensity Factors for β = 1 and α = 0º to 90º

Crack Angle α	Plane Stress Assumption		Plane Strain Assumption	
	$K_I^{(b)}$	$K_{II}^{(b)}$	$K_I^{(b)}$	$K_{II}^{(b)}$
0º	0.00112	0.00121	0.00343	0.00244
15º	0.00484	0.0052	0.0067	0.00643
30º	0.00731	0.00853	0.00818	0.00987
45º	0.00873	0.00916	0.00922	0.00927
60º	0.00532	-0.00541	0.00646	-0.000665
75º	0.00473	-0.00153	0.00536	-0.00323
90º	0.00317	-0.000112	0.00378	-0.000122

Table 6. Membrane Stress Intensity Factors for α =45º and β = 0.05 to 1.6

β	Plane Stress Assumption		Plane Strain Assumption	
	$K_I^{(m)}$	$K_{II}^{(m)}$	$K_I^{(m)}$	$K_{II}^{(m)}$
0.05	0.306	0.364	0.341	0.369
0.1	0.396	0.422	0.427	0.448
0.2	0.474	0.503	0.533	0.527
0.3	0.516	0.574	0.585	0.603
0.4	0.623	0.644	0.655	0.784
0.5	0.712	0.797	0.754	0.823
0.6	0.783	0.877	0.831	0.943
0.75	0.844	0.933	0.893	1.036
0.9	0.923	1.034	1.035	1.143
1.0	1.102	1.16	1.13	1.211
1.15	1.183	1.283	1.231	1.342
1.3	1.294	1.394	1.368	1.421
1.6	1.416	1.473	1.523	1.612

Table 7. Bending Stress Intensity Factors for $\alpha = 45º$ and $\beta = 0.05$ to 1.6

β	Plane Stress Assumption		Plane Strain Assumption	
	$K_I^{(b)}$	$K_{II}^{(b)}$	$K_I^{(b)}$	$K_{II}^{(b)}$
0.05	0.00124	0.00195	0.00194	0.00214
0.1	0.00241	0.00281	0.00312	0.00304
0.2	0.00312	0.00354	0.00394	0.00387
0.3	0.00428	0.00468	0.00502	0.00498
0.4	0.00538	0.00607	0.00617	0.00672
0.5	0.00643	0.00712	0.00684	0.00783
0.6	0.00812	0.00864	0.00881	0.00884
0.75	0.00932	0.00975	0.00974	0.00998
0.9	0.00905	0.00936	0.00947	0.00945
1.0	0.00873	0.00916	0.00922	0.00927
1.15	0.00761	0.00835	0.00789	0.00894
1.3	0.00624	0.00749	0.00716	0.00796
1.6	0.00389	0.00517	0.00546	0.00557